Applications of Skyrme energy-density functional to fusion reactions for synthesis of superheavy nuclei

Ning Wang,[1,*] Xizhen Wu,[2] Zhuxia Li,[2,3,4] Min Liu,[2] and Werner Scheid[1]
[1]*Institute for Theoretical Physics at Justus-Liebig-University, D-35392 Giessen, Germany*
[2]*China Institute of Atomic Energy, Beijing 102413, People's Republic of China*
[3]*Institute of Theoretical Physics, Chinese Academic of Science, Beijing 100080, People's Republic of China*
[4]*Nuclear Theory Center of National Laboratory of Heavy Ion Accelerator, Lanzhou 730000, People's Republic of China*
(Received 12 April 2006; published 16 October 2006)

The Skyrme energy-density functional approach has been extended to study massive heavy-ion fusion reactions. Based on the potential barrier obtained and the parametrized barrier distribution the fusion (capture) excitation functions of a lot of heavy-ion fusion reactions are studied systematically. The average deviations of fusion cross sections at energies near and above the barriers from experimental data are less than 0.05 for 92% of 76 fusion reactions with $Z_1Z_2 < 1200$. For the massive fusion reactions, for example, the ^{238}U-induced reactions and ^{48}Ca + ^{208}Pb, the capture excitation functions have been reproduced remarkably well. The influence of structure effects in the reaction partners on the capture cross sections is studied with our parametrized barrier distribution. By comparing the reactions induced by double-magic nucleus ^{48}Ca and by ^{32}S and ^{35}Cl, the "threshold-like" behavior in the capture excitation function for ^{48}Ca-induced reactions is explored and an optimal balance between the capture cross section and the excitation energy of the compound nucleus is studied. Finally, the fusion reactions with ^{36}S, ^{37}Cl, ^{48}Ca, and ^{50}Ti bombarding ^{248}Cm, ^{247,249}Bk, ^{250,252,254}Cf, and ^{252,254}Es, as well as the reactions leading to the same compound nucleus with $Z = 120$ and $N = 182$, are studied further. The calculation results for these reactions are useful for searching for the optimal fusion configuration and suitable incident energy in the synthesis of superheavy nuclei.

DOI: 10.1103/PhysRevC.74.044604 PACS number(s): 25.60.Pj, 24.10.−i

I. INTRODUCTION

It is of great importance to predict fusion cross sections and to analyze reaction mechanisms for massive heavy-ion fusion reactions, especially for fusion reactions leading to superheavy nuclei. In those reactions, the calculation of the capture cross section is of crucial importance. It is known that Wong's formula [1] based on one-dimensional barrier penetration can describe the fusion excitation function well for light reaction systems; however, it fails to give satisfying results for heavy reaction systems at energies near and below the barrier. To solve this problem, a fusion coupled channel model [2] was proposed, in which the macroscopic Woods-Saxon potential together with a microscopic channel coupling concept was adopted. With this model fusion excitation functions of some reactions at energies near and below the barrier are successfully described. However, it has been found that the parameters in the Woods-Saxon potential greatly influence the results [3] and for heavy systems the potential parameters need to be readjusted to reproduce experimental data [4]. How to determine the parameters is still an unsolved problem in the prediction of fusion cross sections of unmeasured reaction systems. Therefore, it is necessary to propose a new method for systematically describing fusion reactions from light to heavy reaction systems.

In a previous paper [5], we applied the Skyrme energy-density functional for the first time to study heavy-ion fusion reactions. The barrier for fusion reaction was calculated by the Skyrme energy-density functional together with the semiclassical extended Thomas-Fermi method [6]. Based on the interaction potential barrier obtained, we proposed a parametrization of the empirical barrier distribution to take into account the multidimensional character of the real barrier and then applied it to calculate the fusion excitation functions of light and intermediate-heavy fusion reaction systems in terms of the barrier penetration concept. A large number of measured fusion excitation functions at energies around the barriers were reproduced well. Now we try to extend this approach to study very heavy fusion reaction systems that may lead to the formation of superheavy nuclei. In these cases, the reaction mechanism is very complicated: the capture process is the first process involved, followed by the quasifission and fusion, and then the fused system further undergoes fusion-fission and evaporation.

The study of the fusion mechanism (or capture process in very heavy fusion systems), especially of the possible enhancement of the fusion (capture) cross section in neutron-rich reactions and also of the suppression of the capture cross section induced by the strong shell effects of the projectile or the target, is very interesting and essential in the synthesis of superheavy nuclei. For fusion reactions induced by double-magic nucleus ^{48}Ca, there exists a puzzle: on one hand, it has been found that the fusion cross sections at sub-barrier energies are suppressed in fusion reactions ^{48}Ca + ^{48}Ca [7] and ^{48}Ca + ^{90,96}Zr [8,9] compared with ^{40}Ca + ^{48}Ca and ^{40}Ca + ^{90,96}Zr, respectively. On the other hand, the experiments of production of superheavy elements $Z = 114$ and 116 in "hot fusion" reactions with ^{48}Ca bombarding Pu and Cm targets [10] indicate that the reactions with ^{48}Ca nuclei, indeed, are quite

*Electronic address: Ning.Wang@theo.physik.uni-giessen.de

favorable for the synthesis of superheavy nuclei. Therefore, it is worthwhile to explore the puzzle concerning the fusion reactions induced by ^{48}Ca. For this purpose, the influence of shell structure, that is, the influence of the Q-value in the capture process, on the capture cross section is considered in our approach. The choice of an optimal reaction combination and a suitable incident energy is always of crucial importance for the synthesis of new superheavy nuclei. To choose a suitable incident energy, an optimal balance between capture cross section and excitation energy of compound nuclei should be taken into account. Thus, in this work, a series of fusion reactions induced by ^{48}Ca, ^{36}S, ^{37}Cl, and ^{50}Ti is investigated within our approach and the optimal incident energies for the reactions are given.

II. MICROSCOPIC INTERACTION POTENTIAL BARRIER AND PARAMETRIZED BARRIER DISTRIBUTION

In this section, we briefly introduce our approach for calculating the interaction potential barrier and fusion (capture) excitation function, a more detailed description can be found in Ref. [5]. The nucleus-nucleus interaction potentials of fusion systems are calculated within the microscopic Skyrme energy-density functional together with the semiclassical extended Thomas-Fermi (ETF2) approach (up to second order of $\hbar$). The interaction potential $V_b(R)$ between reaction partners can be written as

$$V_b(R) = E_{\text{tot}}(R) - E_1 - E_2, \tag{1}$$

where R is the center-to-center distance between reaction partners, $E_{\text{tot}}(R)$ is the total energy of the interaction system, E_1 and E_2 are the energies of the noninteracting projectile and target, respectively. The interaction potential $V_b(R)$ is also called the entrance-channel potential in Ref. [11] or the fusion potential in Ref. [12]. The $E_{\text{tot}}(R)$, E_1, and E_2 are determined by the Skyrme energy-density functional [6,11,13–15]

$$E_{\text{tot}}(R) = \int \mathcal{H}[\rho_{1p}(\mathbf{r}) + \rho_{2p}(\mathbf{r}-\mathbf{R}), \rho_{1n}(\mathbf{r}) + \rho_{2n}(\mathbf{r}-\mathbf{R})]d\mathbf{r}, \tag{2}$$

$$E_1 = \int \mathcal{H}[\rho_{1p}(\mathbf{r}), \rho_{1n}(\mathbf{r})]\, d\mathbf{r}, \tag{3}$$

$$E_2 = \int \mathcal{H}[\rho_{2p}(\mathbf{r}), \rho_{2n}(\mathbf{r})]\, d\mathbf{r}. \tag{4}$$

Here, ρ_{1p}, ρ_{2p}, ρ_{1n}, and ρ_{2n} are the frozen proton and neutron densities of the projectile and target, and the expression of the energy-density functional $\mathcal{H}$ can be found in Refs. [5,11]. Once the proton and neutron density distributions of the projectile and target are determined, the interaction potential $V_b(R)$ can be calculated from Eqs. (1)–(4).

By using the density-variational approach and minimizing the total energy of a single nucleus given by the Skyrme energy-density functional $\mathcal{H}$, one can obtain the neutron and proton densities of this nucleus. In this work we take the neutron ($i = n$) and proton ($i = p$) density distributions of nuclei as spherical symmetric Fermi functions,

$$\rho_i(\mathbf{r}) = \rho_{0i}\left[1 + \exp\left(\frac{r - R_{0i}}{a_i}\right)\right]^{-1}, \quad i = \{n, p\}. \tag{5}$$

Only two of the three quantities ρ_{0i}, R_{0i}, and a_i in this relation are independent because of the conservation of the particle numbers $N_i = \int \rho_i(\mathbf{r})d\mathbf{r}$, $N_i = \{N, Z\}$. For example, ρ_{0p} can be expressed as a function of R_{0p} and a_p,

$$\rho_{0p} \simeq Z\left\{\frac{4}{3}\pi R_{0p}^3\left[1 + \pi^2\left(\frac{a_p}{R_{0p}}\right)^2\right]\right\}^{-1}, \tag{6}$$

with high accuracy [16] when $R_{0p} \gg a_p$. By using an optimization algorithm, one can obtain the minimal energy and the corresponding R_{0p}, a_p, R_{0n}, and a_n for neutron and proton densities. Then, with the neutron and proton densities of projectile and target obtained one can calculate the entrance-channel potential with the same energy-density functional. To systematically investigate massive heavy-ion fusion reactions with a simple self-consistent manner provided by the density functional theory [17], an optimal balance between the accuracy and computation cost is adopted in this approach, which is especially valuable for theses cases.

The Skyrme force SkM* [15] is adopted in this work. For a certain reaction system, the entrance-channel potential is calculated in a range $R = 7$ to 15 fm with a step size $\Delta R = 0.25$ fm. Figure 1 shows the entrance-channel potential of ^{48}Ca + ^{90}Zr. The solid and crossed curves denote the results of this approach and of the proximity potential [18], respectively. The results of the Skyrme energy-density functional approach are generally close to those of the proximity potential in the region where the densities of the two nuclei does not overlap much. The barrier height B_0, the radius R_0, and the curvature $\hbar\omega_0$ near R_0 as well as the position of fusion pocket R_s can be obtained from the calculations (see Fig. 1). Here, the curvature $\hbar\omega_0$ of the barrier is obtained by fitting the entrance-channel potential in the region from $R_0 - 1.25$ fm to $R_0 + 1.25$ fm by

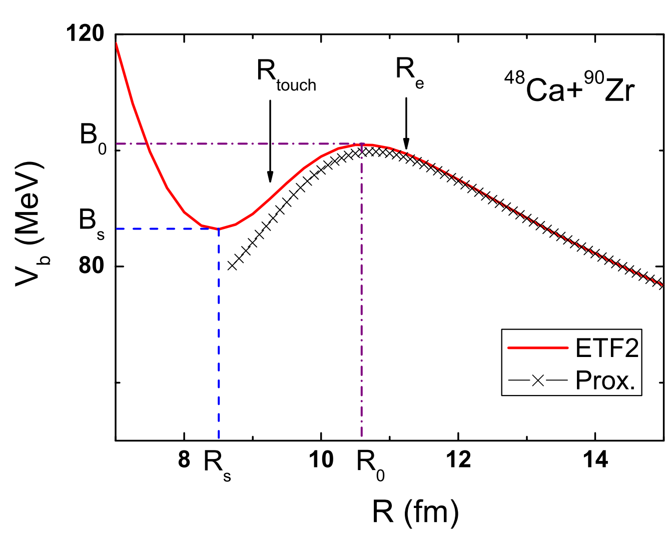

FIG. 1. (Color online) The entrance-channel potential for reaction ^{48}Ca + ^{90}Zr.

an inverted parabola (if $R_0 - 1.25$ fm $< R_s$, then from R_s to $R_0 + 1.25$ fm).

To overcome the deficiency of the one-dimensional barrier penetration model for describing sub-barrier fusion of heavy systems, we take into account the multidimensional character of the realistic barrier [19] due to the coupling to internal degrees of freedom of the binary system. We assume that the one-dimensional barrier is replaced by a distribution of fusion barrier $D(B)$. The distribution function $D(B)$ satisfies

$$\int_0^\infty D(B)\,dB = 1. \tag{7}$$

Motivated by the shape of the barrier distribution extracted from experiments, we consider the weighting function to be a superposition of two Gaussian functions $D_1(B)$ and $D_2(B)$, which read

$$D_1(B) = \frac{\sqrt{\gamma}}{2\sqrt{\pi}w_1}\exp\left[-\gamma\frac{(B-B_1)^2}{(2w_1)^2}\right] \tag{8}$$

and

$$D_2(B) = \frac{1}{2\sqrt{\pi}w_2}\exp\left[-\frac{(B-B_2)^2}{(2w_2)^2}\right], \tag{9}$$

with

$$w_1 = \tfrac{1}{4}(B_0 - B_c), \tag{10}$$
$$w_2 = \tfrac{1}{2}(B_0 - B_c), \tag{11}$$
$$B_1 = B_c + w_1, \tag{12}$$
$$B_2 = B_c + w_2. \tag{13}$$

Here B_0 is the height of the barrier (see Fig. 1). The $B_c = f B_0$ is the effective barrier height with a reducing factor f to mimic the lowering barrier effect that is due to the coupling to other degrees of freedom, such as dynamical deformation and nucleon transfer. We set the reducing factor $f = 0.926$ in this work, which is the same as in [5]. The quantity γ in $D_1(B)$ is a factor to take into account the structure effects, which influence the width of the distribution $D_1(B)$. For the fusion reactions with non-closed-shell nuclei but near the β-stability line we set $\gamma = 1$; for the fusion reactions with neutron-shell-closed nuclei or neutron-rich nuclei an empirical formula for the γ values, used in the weighting function $D_1(B)$ for systems with the same Z_1 and Z_2, was proposed in Ref. [5] as

$$\gamma = 1 - c_0\Delta Q + 0.5\left(\delta_n^{\text{prog}} + \delta_n^{\text{targ}}\right), \tag{14}$$

where $\Delta Q = Q - Q_0$ denotes the difference between the Q-values of the system under consideration for complete fusion and those of the reference system. The reference system, in general, is chosen to be the reaction system with nuclei along the β-stability line [5]. The value of c_0 is 0.5 MeV^{-1} for $\Delta Q < 0$ and 0.1 MeV^{-1} for $\Delta Q > 0$. The quantities $\delta_n^{\text{proj(targ)}}$ are 1 for neutron closed-shell projectile (target) nuclei and 0 for non-closed cases.

The fusion excitation function is then given by

$$\sigma_f(E_{\text{c.m.}}) = \int_0^\infty D(B)\sigma_{\text{fus}}^{\text{Wong}}(E_{\text{c.m.}}, B)\,dB, \tag{15}$$

with

$$\sigma_{\text{fus}}^{\text{Wong}}(E_{\text{c.m.}}, B) = \frac{\hbar\omega_0 R_0^2}{2E_{\text{c.m.}}}\ln\left(1+\exp\left[\frac{2\pi}{\hbar\omega_0}(E_{\text{c.m.}} - B)\right]\right), \tag{16}$$

where $E_{\text{c.m.}}$ denotes the center-of-mass energy, and B, R_0, and $\hbar\omega_0$ are the barrier height, the radius, and the curvature, respectively. Using the parametrized barrier distribution functions $D_1(B)$ and $D_2(B)$, we can also obtain the cross sections $\sigma_1(E_{\text{c.m.}})$ and $\sigma_{\text{avr}}(E_{\text{c.m.}})$ by (15) with $D(B)$ taken to be $D_1(B)$ and $D_{\text{avr}}(B) = [D_1(B) + D_2(B)]/2$, respectively. Finally, the fusion cross section is given by

$$\sigma_{\text{fus}}(E_{\text{c.m.}}) = \min[\sigma_1(E_{\text{c.m.}}), \sigma_{\text{avr}}(E_{\text{c.m.}})]. \tag{17}$$

The cross section calculated with (17) is referred to as the fusion cross section for light and intermediate-heavy systems and as the capture cross section for a very heavy system at $E_{\text{c.m.}}$.

III. CALCULATED RESULTS FOR FUSION (CAPTURE) EXCITATION FUNCTIONS

To extend our approach to study the fusion reactions leading to superheavy nuclei, we first check the suitability and reliability of our description of heavy-ion fusion reactions. We calculate the fusion excitation functions of 76 fusion reactions with $Z_1Z_2 < 1200$ at energies near and above the barrier (with $\gamma = 1$) and their average deviations $\chi^2_{\log}$ from experimental data defined as

$$\chi^2_{\log} = \frac{1}{m}\sum_{n=1}^{m}[\log(\sigma_{\text{th}}(E_n)) - \log(\sigma_{\text{exp}}(E_n))]^2. \tag{18}$$

Here m denotes the number of energy points of experimental data, and $\sigma_{\text{th}}(E_n)$ and $\sigma_{\text{exp}}(E_n)$ are the calculated and experimental fusion cross sections at the center-of-mass energy $E_n (E_n \geqslant B_0)$, respectively. Figure 2 shows the results for $\chi^2_{\log}$ in which the solid circles and crosses denote the calculated results from this approach and those from Ref. [2], respectively.

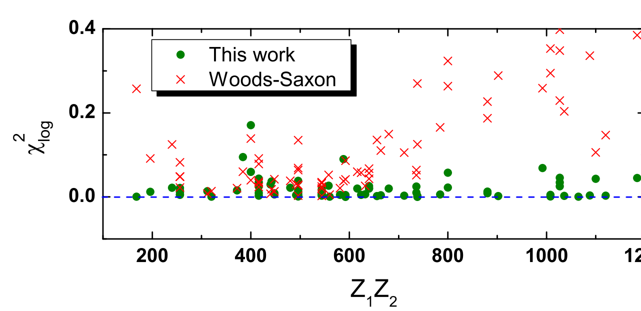

FIG. 2. (Color online) The average deviations $\chi^2_{\log}$ for a total of 76 fusion reactions with $Z_1Z_2 < 1200$. The solid circles and the crosses denote the results of our approach and those with a Woods-Saxon potential with fixed potential parameters [2], respectively. In the calculations of fusion cross sections at energies near and above the barrier with the Woods-Saxon potential, the code CCFULL [2] is used without taking into account the excitation and deformation of the reaction partners.

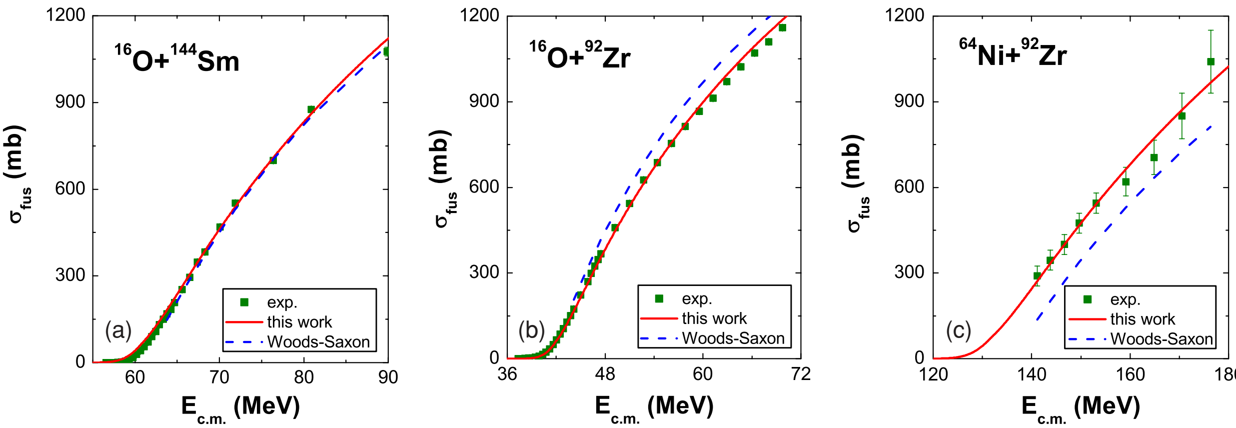

FIG. 3. (Color online) Fusion excitation functions for $^{16}O + ^{144}Sm$, $^{16}O + ^{92}Zr$, and $^{64}Ni + ^{92}Zr$. The squares and solid curves denote the experimental data and the results of this work, respectively. The dashed curves denote the results of the approach with the Woods-Saxon potential with fixed potential parameters [2].

By applying the approach used in Ref. [2], 43% of 76 fusion reactions have average deviations $\chi^2_{\log}$ of calculated fusion cross sections from the experimental data that are less than 0.05, but for reactions with $Z_1Z_2 > 640$ the results are not as satisfying. With our approach, the average deviations of 92% of systems in $\chi^2_{\log}$ are less than 0.05, which indicates that this approach is successful for describing fusion cross sections of heavy-ion reactions at energies near and above the barrier in light to intermediate-heavy fusion systems. In Fig. 3 we show three examples of fusion excitation functions for the reactions $^{16}O + ^{144}Sm$ [20], $^{16}O + ^{92}Zr$ [21], and $^{64}Ni + ^{92}Zr$ [22], in which the solid and dashed curves present the results of our approach and those of Ref. [2], respectively. The squares denote the experimental data. From this figure we can see that our approach gives quite a reasonable description for all selected fusion reactions with the Z_1Z_2 up to 1120 at energies near and above the barrier.

For more massive fusion reactions leading to superheavy nuclei, the quasifission process occurs and, therefore, the capture cross sections are larger than the corresponding fusion cross sections. In Ref. [23] the fission and quasifission processes in ^{238}U-induced reactions were studied. Figure 4 shows the results; the solid and open circles denote the measured cross sections for the fission-like process and for complete fusion followed by fission, respectively. The solid curves give the calculated results of our approach with $\gamma = 1$. From this figure one can see that the calculated capture excitation functions of the reactions $^{238}U + ^{26}Mg$, $^{238}U + ^{27}Al$, $^{238}U + ^{32}S$, and $^{238}U + ^{35}Cl$ are quite close to the measured fission-like cross sections. It implies that our approach can describe the massive fusion reactions between nuclei with neutron open shells but near the β-stability line.

For the very massive fusion reactions between double-magic nuclei ^{48}Ca and ^{208}Pb, the influence of the shell effects is very significant. So careful consideration of the γ value is required at sub-barrier energies. Figure 5 shows the calculated capture excitation function of $^{48}Ca + ^{208}Pb$ and the experimental data of Refs. [25] and [26]. The dashed curve represents the results with $\gamma = 1$; that is, no neutron-shell-closure effect is considered. The solid curve is calculated with $\gamma = 9.5$ according to Eq. (14), in which the closed shell effect is considered. We find that for energies below the barrier the experimental data can only be described with $\gamma = 9.5$ and the calculations with $\gamma = 1$ are overpredicted. From this analysis, one learns that the measured capture cross sections of $^{48}Ca + ^{208}Pb$ at sub-barrier energies are obviously suppressed, which may arise from the suppression of the nucleon transfer between reaction partners due to the strong closed shell effects, which are further studied in the following section.

IV. OPTIMAL BALANCE BETWEEN CAPTURE CROSS SECTION AND EXCITATION ENERGY OF COMPOUND NUCLEI

It is very important to find a favorable combination of projectile and target and a suitable incident energy for synthesis of superheavy nuclei. In this section we study very massive fusion reactions and search for an optimal balance between the capture cross section in the entrance channel and the excitation energy of the compound nuclei. To search a fusion system with large capture cross sections, we carried out a series of calculations for fusion reactions induced by ^{32,36}S, ^{35,37}Cl, and ^{48}Ca projectiles. For example, Fig. 6 shows the capture excitation functions of the reactions $^{32}S + ^{254}Cf$ and $^{35}Cl + ^{254}Es$. The solid curves present the results with $\gamma = 1$ (without considering structure effects in the entrance channel), and the dashed curves are for the results with the γ obtained from (14), i.e., $\gamma = 0.5$ for $^{32}S + ^{254}Cf$ and $\gamma = 0.6$ for $^{35}Cl + ^{254}Es$. The enhancement of capture cross sections in the sub-barrier energy region with the $\gamma < 1$ is caused by the effect of an excess of neutrons in the reaction systems. So from the point of view of increasing the capture cross sections, it is more favorable to select the reaction systems with $\gamma < 1$. However, the amount of the excitation energy of the formed compound nucleus is essential for the survival probability. The smaller the excitation energy is, the larger the surviving probability is. Thus, seeking an optimal balance between the capture cross section and the excitation energy of the compound nucleus becomes very important for synthesis

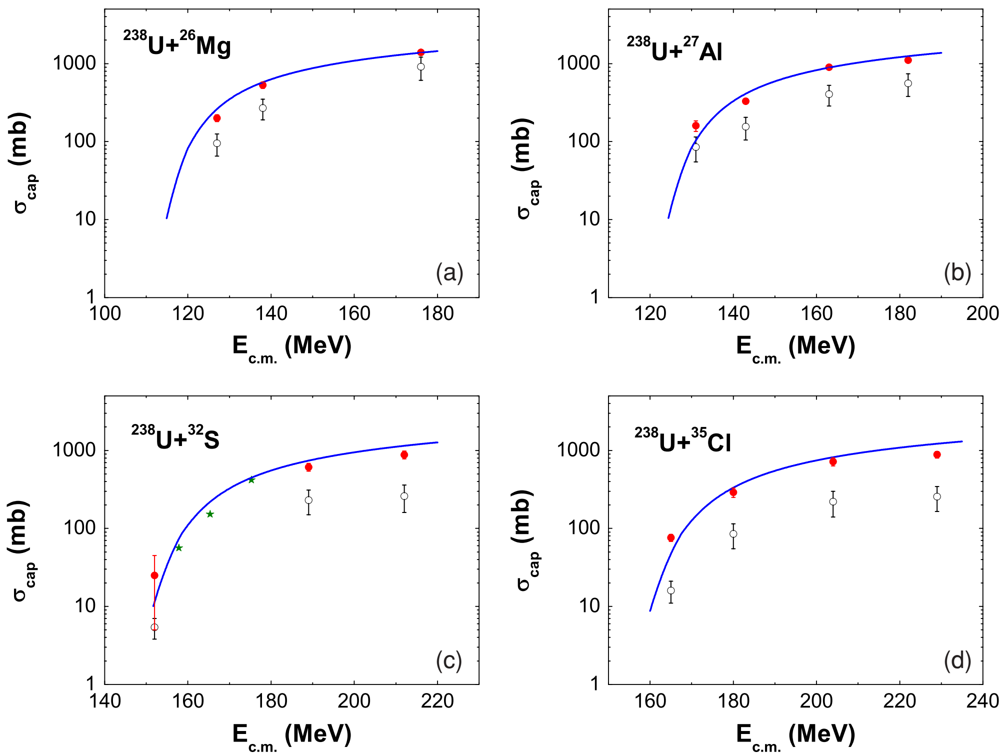

FIG. 4. (Color online) Capture cross sections of ^{238}U + ^{26}Mg, ^{27}Al,^{32}S, and ^{35}Cl. The solid and open circles denote the measured cross sections for a fission-like process and for complete fusion followed by fission, respectively. The solid curves are the results from our approach with $\gamma = 1$. The stars are taken from Ref. [24].

of superheavy nuclei. For choosing the fused nuclei with an excitation energy as low as possible, the fusion reactions with double-magic nuclei ^{48}Ca are considered to be good candidates because of the low Q values for those fusion reactions. As an example, let us investigate reaction ^{48}Ca + ^{248}Cm. For this reaction the γ value is equal to 10.8, calculated with

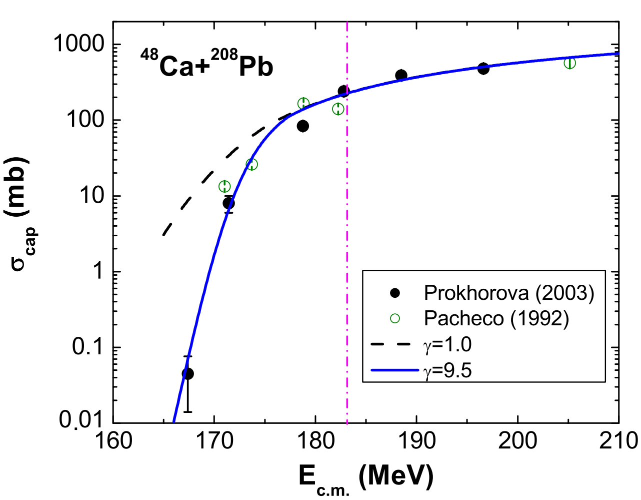

FIG. 5. (Color online) Capture cross sections of ^{48}Ca + ^{208}Pb. The solid and open circles denote the measured capture-fission cross sections from Refs. [25] and [26], respectively. The dashed and solid curves represent the results calculated with $\gamma = 1.0$ and 9.5, respectively, obtained by Eq. (14). The dash-dotted line indicates the energy corresponding to the height of the barrier.

Eq. (14). Figure 7 shows the capture excitation function for this reaction, in which the solid and dashed curves denote the results for the cases of $\gamma = 1$ and $\gamma = 10.8$, respectively. From this figure one finds that for fusion reactions induced by double-magic nuclei ^{48}Ca the capture cross sections at sub-barrier energies are suppressed compared with reactions with open-shell nuclei but near the β-stability line. However, if we suitably choose an incident energy, for example, as indicated by the arrow in Fig. 7, the capture cross section of the reaction ^{48}Ca + ^{248}Cm is not suppressed so much (still reaches several tens of millibarns) and the excitation energy of the compound nuclei is only $E^*_{\rm CN} = 31$ MeV. Such an incident energy was already used in the experiment in Ref. [10]. Now let us make a comparison between the reaction ^{48}Ca + ^{248}Cm and the reactions ^{32}S + ^{254}Cf and ^{35}Cl + ^{254}Es. For the system ^{48}Ca + ^{248}Cm, the capture cross section is about 80 mb and the excitation energy is about 31 MeV if the incident energy is taken to be about 198 MeV. While, for the systems ^{32}S + ^{254}Cf and ^{35}Cl + ^{254}Es, if the same excitation energy is required the incident energies must be as low as about 150 and 160 MeV, respectively, because the Q values of these two fusion reactions are much higher compared with those of ^{48}Ca-induced reactions. At these incident energies the capture cross sections for these two reactions are as small as those less than 0.1 mb according to this model's calculations. From the previous analysis we can conclude that the fusion reaction ^{48}Ca + ^{248}Cm seems to be more favorable compared to ^{32}S + ^{254}Cf and ^{35}Cl + ^{254}Es if a suitable incident energy is chosen, as far as both the capture cross section and the excitation energy of the compound nuclei are concerned.

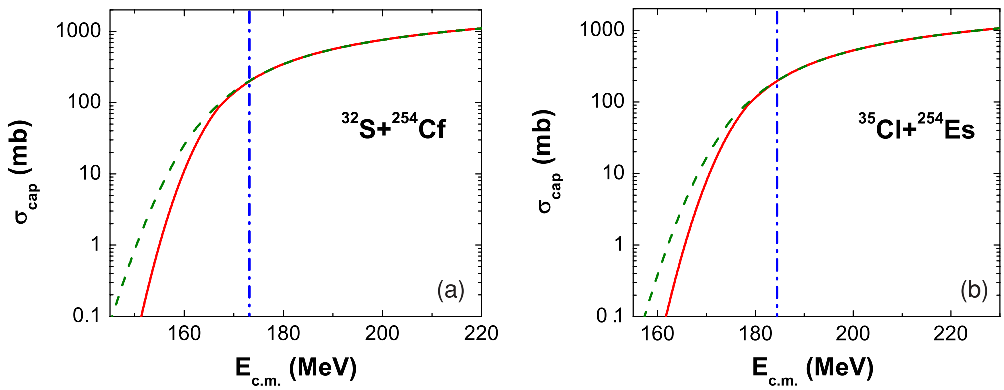

FIG. 6. (Color online) Capture excitation functions for fusion systems $^{32}S + ^{254}Cf$ and $^{35}Cl + ^{254}Es$. The dash-dotted lines indicate the corresponding barriers. The solid and dashed curves denote the results with $\gamma = 1$ and with the γ value obtained with Eq. (14), respectively.

Now let us discuss how to choose a suitable incident energy. We notice that the capture excitation function for reactions induced by double-magic ^{48}Ca goes very sharply down at sub-barrier energies due to strong closed shell effects, as shown by the dashed curve of Fig. 7. It seems to us that there exists a threshold-like behavior that is important for choosing the incident energies. This threshold-like behavior of the excitation function of capture cross sections is closely related to the shape of the barrier distribution. In our previous paper [5], a number of barrier distributions were calculated according to expressions (8)–(13). For example, here we show the calculated fusion barrier distribution for $^{16}O + ^{208}Pb$ [27] in Fig. 8. The agreement of the calculated barrier distribution data with the experimental data tells us that our approach to the parametrized barrier distribution is quite reasonable. The effective weighting function $D_{\rm eff}(B)$ is defined as

$$D_{\rm eff}(B) = \begin{cases} D_1(B) & : \quad B < B_x \\ D_{\rm avr}(B) & : \quad B \geqslant B_x \end{cases} \qquad (19)$$

(with $\int D_{\rm eff}(B)\,dB \approx 1$ and $\int D_{\rm avr}(B)\,dB = 1$, see Ref. [5]). The B_x denotes the position of the left crossing point between $D_1(B)$ and $D_{\rm avr}(B)$. The function $D_{\rm eff}(B)$ can describe the fusion excitation function reasonably well. Figure 9 shows the capture excitation function [Fig. 9(a)] and the effective weighting function $D_{\rm eff}$ [Fig. 9(b)] for the reaction $^{48}Ca + ^{244}Pu$. The dotted vertical line denotes the barrier height B_0, and the short dashed vertical line indicates the energy at the peak of $D_{\rm eff}$ that we call the most probable barrier height $B_{\rm m.p.}$. From the dashed curve of Fig. 9(a) one can see that the capture cross section goes down very sharply when the incident energy is lower than $B_{\rm m.p.}$. This is because the decreasing slope of the left side of the weighting function $D_{\rm eff}$ is very steep because of strong closed shell effects ($\gamma = 11.0$). In fact, one can find that the left side of the barrier distribution $D_{\rm eff}(B)$ is given by $D_1(B)$ [see expression (19)], which becomes a δ function when $\gamma \to \infty$. For the system with γ much larger than 1 the effective barrier $D_{\rm eff}$ has a similar behavior as is shown in Fig. 9(b). Thus, the most probable barrier energy

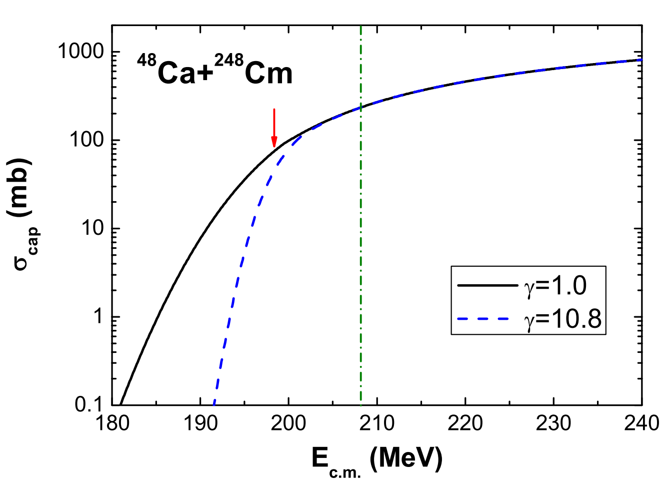

FIG. 7. (Color online) Capture excitation functions for $^{48}Ca + ^{248}Cm$. The solid and dashed curves represent the results with $\gamma = 1$ and with $\gamma = 10.8$ obtained from Eq. (14). The arrow indicates the incident energy at which the corresponding excitation energy of the formed compound nucleus is $E^*_{\rm CN} = 31$ MeV.

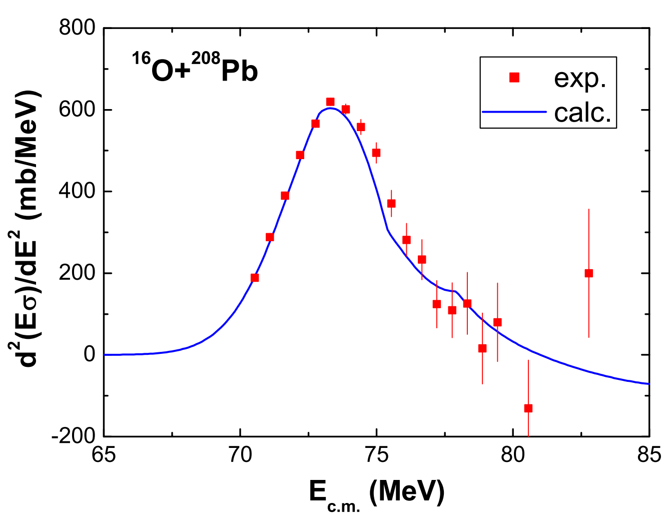

FIG. 8. (Color online) Fusion barrier distribution for $^{16}O + ^{208}Pb$. The distribution is evaluated with $\Delta E_{\rm c.m.} = 2.5$ MeV. The solid squares and solid curve represent the experimental data and the results from our calculations, respectively.

TABLE I. The entrance-channel capture barriers of fusion reactions with ^{48}Ca nuclei.

Reaction	B_0(MeV)	R_0(fm)	$\hbar\omega_0$(MeV)	γ	B_{mean}(MeV)	$B_{\text{m.p.}}$(MeV)	$E_{\text{min}}^{\text{exp}}$(MeV)
^{48}Ca+^{207}Pb [28]	183.37	12.0	4.44	8.9	176.28	173.18	173.3
^{48}Ca+^{208}Pb [28]	183.17	12.0	4.43	9.5	176.10	173.03	173.5
^{48}Ca+^{238}U [29]	200.82	12.25	4.19	10.7	193.09	189.71	191.1
^{48}Ca+^{242}Pu [29]	204.78	12.25	3.90	11.6	196.91	193.44	196
^{48}Ca+^{244}Pu [30]	204.31	12.25	3.99	11.0	196.44	192.99	193.3
^{48}Ca+^{243}Am [31]	206.87	12.25	3.87	9.8	198.89	195.39	207.1
^{48}Ca+^{245}Cm [30]	208.80	12.25	3.88	11.7	200.77	197.22	203
^{48}Ca+^{248}Cm [29]	208.25	12.25	3.89	10.8	200.23	196.71	198.6

$B_{\text{m.p.}}$ can be considered as the incident energy "threshold," and for massive fusion reactions with γ much larger than 1 leading to superheavy nuclei such as ^{48}Ca-induced reactions, the suitable incident energy should be chosen in the region $E_{\text{c.m.}} > B_{\text{m.p.}}$. The barrier distribution for this case shown in Fig. 9(b) looks like a δ function with a long tail in the high energy side. It seems that Wong's formula with barrier height being the $B_{\text{m.p.}}$ should work without introducing the γ. But the results calculated with Wong's formula and expression (17) are different especially at sub-barrier energies, as shown in Fig. 9(a) (compare the dot-dashed curve and the dashed curve). It seems to us that with a γ value like $\gamma = 11.0$ the behavior of D_{eff} is still different from a that of a δ function and the parameter γ still plays a role.

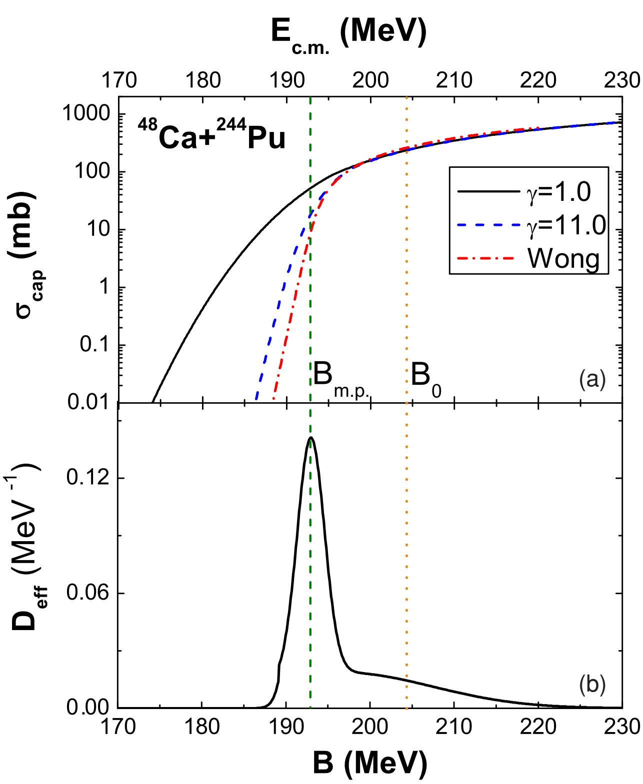

FIG. 9. (Color online) (a) Capture excitation function and (b) effective weighting function for the reaction ^{48}Ca + ^{244}Pu. In (a) the solid and dashed curves show the results with $\gamma = 1$ and with γ obtained by Eq. (14), respectively. The dot-dashed curve denotes the results from Wong's formula with $B = B_{\text{m.p.}}$. The results in (b) are obtained by setting $\gamma = 11.0$.

We find that the incident energies adopted in the experiments successfully producing superheavy nuclei in recent years [28–31] for some reactions induced by ^{48}Ca are very close the most probable barrier energies $B_{\text{m.p.}}$. Table I gives the comparison of the calculated most probable barrier energies $B_{\text{m.p.}}$ with the minimal experimental incident energies $E_{\text{min}}^{\text{exp}}$ used in Refs. [28–31] for some reactions induced by ^{48}Ca leading to the production of superheavy nuclei. The barrier height B_0, the position R_0 of the barrier, the curvature at the top of the barrier expressed by $\hbar\omega_0$, and factor γ are also listed. In addition, we list the mean value B_{mean} of the barrier height defined as

$$B_{\text{mean}} = \frac{\int B\, D_{\text{eff}}(B)\, dB}{\int D_{\text{eff}}(B)\, dB}. \tag{20}$$

The B_{mean} is, in general, larger than the $B_{\text{m.p.}}$ because the slope of the left side of the weighting function D_{eff} is very steep. From Table I one can find that for all listed reactions the energies $E_{\text{min}}^{\text{exp}}$ are higher than the calculated most probable barrier energies $B_{\text{m.p.}}$, which supports our ideas about how to choose a favorable incident energy. Further, we find that the experimental evaporation-residue excitation functions of the fusion reactions listed in Table I are peaked at the energies ranging from B_{mean} to B_0 in most cases, which implies that the energy B_{mean} may be more suitable to be chosen as the incident beam energy in the fusion reactions with γ much larger than 1 for producing superheavy nuclei.

In addition to the reactions induced by ^{48}Ca leading to superheavy nuclei, reactions with ^{36}S, ^{37}Cl, ^{48}Ca, and ^{50}Ti bombarding ^{248}Cm, ^{247,249}Bk, ^{250,252,254}Cf, and ^{252,254}Es are also studied and all relevant parameters for the entrance-channel capture barriers for those fusion reactions are listed in Table II. The table gives the Q value for the reactions, the barrier height B_0, the position R_0 of the barrier, the curvature at the top of the barrier expressed by $\hbar\omega_0$, factor γ of structure effects, the mean value B_{mean} of the barrier, the most probable barrier energy $B_{\text{m.p.}}$, the excitation energy of compound nucleus E_{CN}^* when $E_{\text{c.m.}} = B_{\text{mean}}$, and the depth of the capture pocket $B_0 - B_s$ (also called quasifission barrier height [32], here B_s denotes the value at the bottom of the pocket, see Fig. 1). Comparing the data from different reactions one can find that the reactions with ^{37}Cl induce relatively higher excitation energies E_{CN}^* and those with ^{48}Ca

TABLE II. The entrance-channel capture barriers for fusion reactions with ^{36}S, ^{37}Cl, ^{48}Ca, and ^{50}Ti bombarding ^{248}Cm, ^{247,249}Bk, ^{250,252,254}Cf, and ^{252,254}Es.

Reaction	Q(MeV)	B_0(MeV)	R_0(fm)	$\hbar\omega_0$(MeV)	γ	B_{mean}(MeV)	$B_{\text{m.p.}}$(MeV)	E^*_{CN}(MeV)	$B_0 - B_s$
^{36}S+^{248}Cm	−122.05	170.45	12.0	4.34	5.3	163.75	161.00	41.70	8.72
^{36}S+^{247}Bk	−126.30	172.60	12.0	4.33	4.7	165.78	163.10	39.48	8.43
^{36}S+^{249}Bk	−124.58	172.03	12.0	4.23	3.9	165.18	162.58	40.60	8.23
^{36}S+^{250}Cf	−127.14	174.04	12.0	4.29	6.2	167.24	164.37	40.10	8.27
^{36}S+^{252}Cf	−125.00	173.53	12.0	4.23	5.1	166.70	163.89	41.70	8.41
^{36}S+^{254}Cf	−122.48	173.02	12.0	4.17	3.9	166.13	163.51	43.65	8.49
^{36}S+^{252}Es	−128.84	175.36	12.0	4.23	5.4	168.47	165.65	39.63	8.18
^{36}S+^{254}Es	−126.81	174.97	12.0	4.17	4.4	168.04	165.26	41.23	8.25
^{37}Cl+^{248}Cm	−128.14	180.65	12.25	4.58	3.0	173.37	170.66	45.23	7.86
^{37}Cl+^{247}Bk	−131.56	182.90	12.0	4.25	2.8	175.50	172.83	43.94	7.46
^{37}Cl+^{249}Bk	−129.56	182.60	12.25	4.54	1.8	175.03	172.61	45.47	7.59
^{37}Cl+^{250}Cf	−134.39	184.45	12.25	4.55	4.1	177.12	174.28	42.73	7.35
^{37}Cl+^{252}Cf	−131.94	184.03	12.25	4.54	2.9	176.60	173.87	44.65	7.56
^{37}Cl+^{254}Cf	−129.40	183.57	12.25	4.52	1.6	175.91	173.53	46.52	7.74
^{37}Cl+^{252}Es	−135.20	185.96	12.25	4.54	3.5	178.51	175.70	43.31	7.23
^{37}Cl+^{254}Es	−132.96	185.62	12.25	4.52	2.4	178.04	175.44	45.08	7.41
^{48}Ca+^{248}Cm	−167.27	208.25	12.25	3.89	10.8	200.23	196.71	32.96	5.46
^{48}Ca+^{247}Bk	−171.71	210.80	12.25	3.95	9.6	202.67	199.11	30.95	5.27
^{48}Ca+^{249}Bk	−170.76	210.46	12.25	3.83	9.1	202.33	198.76	31.57	5.30
^{48}Ca+^{250}Cf	−174.53	212.56	12.25	3.66	11.4	204.39	200.81	29.86	5.11
^{48}Ca+^{252}Cf	−173.77	212.10	12.5	4.41	11.0	203.94	200.37	30.17	5.17
^{48}Ca+^{254}Cf	−173.28	211.63	12.5	4.38	10.7	203.48	199.92	30.20	5.25
^{48}Ca+^{252}Es	−177.43	214.29	12.5	4.43	10.6	206.04	202.39	28.61	4.98
^{48}Ca+^{254}Es	−176.97	213.94	12.5	4.39	10.3	205.70	202.13	28.73	5.05
^{50}Ti+^{248}Cm	−185.52	229.00	12.25	3.75	3.9	219.88	216.39	34.36	4.41
^{50}Ti+^{247}Bk	−191.42	231.85	12.25	3.80	4.1	222.63	219.00	31.21	4.14
^{50}Ti+^{249}Bk	−189.78	231.45	12.25	3.67	3.3	222.16	218.71	32.38	4.18
^{50}Ti+^{250}Cf	−194.40	233.79	12.25	3.64	4.9	224.56	220.84	30.16	3.98
^{50}Ti+^{252}Cf	−193.02	233.23	12.25	3.53	4.2	223.97	220.33	30.95	3.96
^{50}Ti+^{254}Cf	−191.92	232.67	12.5	4.38	3.6	223.38	219.81	31.46	3.97
^{50}Ti+^{252}Es	−197.90	235.72	12.25	3.52	4.3	226.37	222.67	28.47	3.71
^{50}Ti+^{254}Es	−196.81	235.24	12.5	4.39	3.8	225.86	222.21	29.05	3.69

and ^{50}Ti produce relatively lower excitation energies when $E_{\text{c.m.}} = B_{\text{mean}}$. So ^{48}Ca- and ^{50}Ti-induced reactions can be considered as good candidates of cold fusion reaction for producing superheavy nuclei from the point of a low excitation energy of the compound nuclei. Here we have not studied the orientation effect of deformed targets, which has significant effects on the fusion barrier height and the compactness of the fusion reactions. Recently, the compactness of ^{48}Ca-induced hot fusion reactions was studied and it was shown that ^{48}Ca-induced reactions on various actinides were the

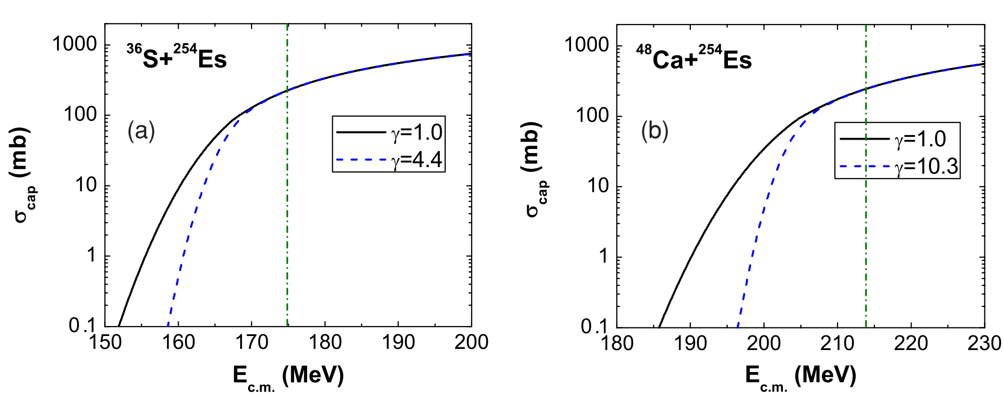

FIG. 10. (Color online) Capture excitation functions for the systems (a) ^{36}S + ^{254}Es and (b) ^{48}Ca + ^{254}Es.

TABLE III. The same as Table II, but for reactions $^{64}Ni + ^{238}U$, $^{58}Fe + ^{244}Pu$, $^{54}Cr + ^{248}Cm$, and $^{50}Ti + ^{252}Cf$.

Reaction	Q(MeV)	B_0(MeV)	R_0(fm)	$\hbar\omega_0$(MeV)	γ	B_{mean}(MeV)	$B_{m.p.}$(MeV)	E^*_{CN}(MeV)	$B_0 - B_s$
$^{64}Ni+^{238}U$	−237.41	276.01	12.5	4.61	7.1	265.26	260.73	27.85	1.79
$^{58}Fe+^{244}Pu$	−219.97	262.88	12.25	3.93	1.0	251.56	248.80	31.60	2.56
$^{54}Cr+^{248}Cm$	−207.16	248.52	12.25	4.20	3.0	238.51	234.86	31.35	3.26
$^{50}Ti+^{252}Cf$	−193.02	233.23	12.25	3.53	4.2	223.97	220.33	30.95	3.96

best cold fusion reactions with optimum orientations of the hot fusion process [33]. By comparing the depths of the capture pockets for different reactions we find that the depth decreases with increase of the proton number of the projectile nuclei. We know that the shallower the pocket is, the stronger the quasifission is. So the projectile ^{36}S inducing capture reactions is more favorable for the small quasifission probabilities of those reactions. By using Table II we can easily calculate the capture cross sections by using Eqs. (15)–(17) for all the reactions listed. Figure 10 shows the calculated capture excitation functions for the systems $^{36}S + ^{254}Es$ and $^{48}Ca + ^{254}Es$ with our approach by using the data from Table II. In addition, the entrance-channel capture barriers of the reactions $^{64}Ni + ^{238}U$, $^{58}Fe + ^{244}Pu$, $^{54}Cr + ^{248}Cm$, and $^{50}Ti + ^{252}Cf$ that lead to the same compound nucleus with $Z = 120$ and $N = 182$ are calculated and listed in Table III. Tables II and III provide us with very useful information for choosing an optimal combination of projectile and target and suitable incident beam energies for producing superheavy nuclei for unmeasured massive fusion reactions.

V. CONCLUSION AND DISCUSSION

In this work, the Skyrme energy-density functional approach was applied to study massive heavy-ion fusion reactions, especially those leading to superheavy nuclei. Based on the barriers calculated with the Skyrme energy-density functional, we propose the parametrized barrier distributions to effectively take into account the multidimensional character of the realistic barrier. A large number of heavy-ion fusion reactions were studied systematically. The average deviations of fusion cross sections at energies near and above the barriers from experimental data are less than 0.05 for 92% of 76 fusion reactions with $Z_1Z_2 < 1200$. Massive fusion reactions, for example, the ^{238}U-induced reactions and the $^{48}Ca + ^{208}Pb$ reaction were studied and their capture excitation functions were reproduced well. The influence of the structure effects in the reaction partners on the capture cross sections is studied by using parameter γ in our model. To search the most favorable condition for the synthesis of superheavy nuclei, the optimal balance between the capture cross section and the excitation energy of the formed compound nuclei was studied by comparing the fusion reactions induced by the double-magic nucleus ^{48}Ca and by ^{32}S and ^{35}Cl. Based on this study, the threshold-like behavior of the excitation function of capture cross sections with respect to incident beam energy was explored and possible values of this threshold for reactions mainly induced by ^{48}Ca are given. Finally, we further studied the capture reactions leading to superheavy nuclei such as ^{36}S, ^{37}Cl, ^{48}Ca, and ^{50}Ti bombarding ^{248}Cm, $^{247,249}Bk$, $^{250,252,254}Cf$, and $^{252,254}Es$, as well as the reactions $^{64}Ni + ^{238}U$, $^{58}Fe + ^{244}Pu$, $^{54}Cr + ^{248}Cm$, and $^{50}Ti + ^{252}Cf$ which lead to the same compound nucleus with $Z = 120$ and $N = 182$. The relevant parameters for calculating the capture cross sections of these reactions have been provided, which is helpful for the study of unmeasured massive fusion reactions. Especially, we predicted optimal fusion configuration and suitable incident beam energies for the synthesis of superheavy nuclei.

We notice that the deformation and orientation of colliding nuclei has a very significant role in fusion reactions. In Refs. [34,35], the effect of deformation and orientation on the barrier hight and the compactness of fusion reactions was investigated systematically. However, this kind study is beyond the scope of the present work. We have only made preliminary calculations of the potential barrier for $^{48}Ca + ^{248}Cm$ with the deformation and orientation of ^{248}Cm taken into account in the entrance channel. For this reaction the lowest barrier is obtained for the orientation $\Theta = 0^\circ$, i.e., when ^{48}Ca touches the tip of the deformed ^{248}Cm target; whereas the highest barrier is obtained for $\Theta = 90^\circ$, when ^{48}Ca touches the side. The lowest barrier obtained for $\Theta = 0^\circ$ is a little bit lower than the most probable barrier height $B_{m.p.}$ of this reaction given in Table I and the barrier distribution due to the orientation of ^{248}Cm is close to the effective weighting function $D_{eff}(B)$ which is for describing the capture process of the reaction if assuming the orientation probability decreases gradually from 0° to 90°. So the deformation effects seem to be partly involved in the parametrized barrier distribution functions. The study of this aspect is in progress.

ACKNOWLEDGMENTS

Wang is grateful to Professor Enguang Zhao and Professor Junqing Li for fruitful discussions. This work was supported by the Alexander von Humboldt Foundation and the National Natural Science Foundation of China, Nos. 10235030 and 10235020.

[1] C. Y. Wong, Phys. Rev. Lett. **31**, 766 (1973).
[2] K. Hagino, N. Rowley, and A. T. Kruppa, Comput. Phys. Commun. **123**, 143 (1999).
[3] J. O. Newton, R. D. Butt, M. Dasgupta, D. J. Hinde, I. I Gontchar, C. R. Morton, and K. Hagino, Phys. Rev. C **70**, 024605 (2004).

[4] K. Siwek-Wilczyńska and J. Wilczyński, Phys. Rev. C **69**, 024611 (2004).
[5] M. Liu, N. Wang, Z. Li, X. Wu, and E. Zhao, Nucl. Phys. **A768**, 80 (2006).
[6] M. Brack, C. Guet, and H.-B. Hakanson, Phys. Rep. **123**, 275 (1985).
[7] M. Trotta, A. M. Stefanini, L. Corradi, A. Gadea, F. Scarlassara, S. Beghini, and G. Montagnoli, Phys. Rev. C **65**, 011601(R) (2002).
[8] A. M. Stefanini, F. Scarlassara *et al.*, Phys. Rev. C **73**, 034606 (2006).
[9] Huanqiao Zhang *et al.* Chin. Phys. Lett. **22**, 3048 (2005).
[10] Yu. Ts. Oganessian, V. K. Utyonkov, Yu. V. Lobanov *et al.*, Phys. Rev. C **62**, 041604(R) (2000); **63**, 011301(R) (2001).
[11] V. Yu. Denisov and W. Noerenberg, Eur. Phys. J. A **15**, 375 (2002).
[12] R. Bass, Nucl. Phys. **A231**, 45 (1974).
[13] D. Vautherin and D. M. Brink, Phys. Rev. C **5**, 626 (1972).
[14] J. Bartel and K. Bencheikh, Eur. Phys. J. A **14**, 179 (2002).
[15] J. Bartel, M. Brack, and M. Durand, Nucl. Phys. **A445**, 263 (1985).
[16] B. Grammaticos, Z. Phys. A **305**, 257 (1982).
[17] P. Hohenberg and W. Kohn, Phys. Rev. **136**, B864 (1964).
[18] W. D. Myers and W. J. Światecki, Phys. Rev. C **62**, 044610 (2000).
[19] P. H. Stelson, Phys. Lett. **B205**, 190 (1988).
[20] J. R. Leigh, M. Dasgupta, and D. J. Hinde, Phys. Rev. C **52**, 3151 (1995).
[21] J. O. Newton, C. R. Morton, M. Dasgupta, J. R. Leigh, J. C. Mein, D. J. Hinde, H. Timmers, and K. Hagino, Phys. Rev. C **64**, 64608 (2001).
[22] F. L. H. Wolfs, R. V. F. Janssens, R. Holzmann, T. L. Khoo, W. C. Ma, and S. J. Sanders, Phys. Rev. C **39**, 865 (1989).
[23] W. Q. Shen, J. Albinski, A. Gobbi *et al.*, Phys. Rev. C **36**, 115 (1987).
[24] J. Toke, R. Bock *et al.*, Phys. Lett. **B142**, 258 (1984).
[25] E. V. Prokhorova, E. A. Cherepanov, M. G. Itkis *et al.*, arXiv:nucl-ex/0309021.
[26] A. J. Pacheco, J. O. Fernandez Niello, D. E. DiGregorio, M. diTada, J. E. Testoni, Y. Chan, E. Chavez, S. Gazes, E. Plagnol, and R. G. Stokstad, Phys. Rev. C **45**, 2861 (1992).
[27] C. R. Morton, A. C. Berriman, M. Dasgupta, D. J. Hinde, J. O. Newton, K. Hagino, and I. J. Thompson, Phys. Rev. C **60**, 044608 (1999).
[28] Yu. Ts. Oganessian, V. K. Utyonkov, Yu. V. Lobanov *et al.*, Phys. Rev. C **64**, 054606 (2001).
[29] Yu. Ts. Oganessian, V. K. Utyonkov, Yu. V. Lobanov *et al.*, Phys. Rev. C **70**, 064609 (2004).
[30] Yu. Ts. Oganessian, V. K. Utyonkov, Yu. V. Lobanov *et al.*, Phys. Rev. C **69**, 054607 (2004).
[31] Yu. Ts. Oganessian, V. K. Utyonkov, Yu. V. Lobanov *et al.*, Phys. Rev. C **69**, 021601 (2004).
[32] G. G. Adamian, N. V. Antonenko, W. Scheid, and V. V. Volkov, Nucl. Phys. **A627**, 361 (1997).
[33] R. K. Gupta, M. Manhas, and W. Greiner, Phys. Rev. C **73**, 054307 (2006).
[34] A. Iwamoto, P. Möller, J. R. Nix, and H. Sagawa, Nucl. Phys. **A596**, 329 (1996).
[35] R. K. Gupta *et al.*, J. Phys. G: Nucl. Phys. **31**, 631 (2005).